Characterization of the pressure fluctuations within a Controlled-Diffusion airfoil boundary layer at large Reynolds numbers

R. Boukharfane [*], J. Bodart [†], M.C. Jacob [‡], and L. Joly [§]
ISAE-Supaero, BP 54032, 31055 Toulouse Cedex 04, France

T. Bridel-Bertomeu [¶],
French Alternative Energies and Atomic Energy Commission (CEA), Bordeaux, France

T. Nodé-Langlois [‖]
Acoustics Methods, Airbus Commercial Aircraft, Toulouse, France

The present investigation targets the generation of airfoil trailing-edge broadband noise that arises from the interaction of turbulent boundary layer with the airfoil trailing edge. Large-eddy simulations, carried out using a massively parallel compressible solver CharLES^X, are conducted for a Controlled-Diffusion (CD) airfoil with rounded trailing edge for seven configurations, characterized with a Reynolds number, angle of attack and Mach number. An analysis of the unsteady pressure signals in the boundary layer is proposed in regard to classical trailing edge noise modelling ingredients.

Introduction

IN today's context of increasing oil prices and environmental awareness, aerospace companies are once again looking at CROR (Contra-Rotating Open Rotor) and UHBR fan (Ultra High By-pass Ratio) technologies for single-aisle aircrafts. With very large by-pass ratio and by reducing both the nitrous oxides and the dioxide carbon emissions, they promise a significant increase in fuel efficiency and represent a potential power-plant for future commercial transport aircraft. However, one of the major problems for public acceptance of such technologies is the noise radiated by aircraft engines.

It is widely accepted that the broadband noise induced by the interaction of the boundary layer with the airfoil trailing edge (TE), known as the turbulent boundary layer TE noise, plays a significant role in the overall airframe noise. To achieve the challenging objective of reducing this source of noise, the first important thing is to propose an accurate methodology for TE noise prediction. This can be done using three distinct methods: semi-empirical, direct and hybrid methods. As the semi-empirical models are based on a set of experimental data, their accuracy and applicability is still questionable and limited since the models are calibrated against experimental data which can lead to poor prediction for other airfoil profiles and flow conditions [1]. The direct methods have the ability to provide accurate and reliable predictions and are applicable to industrial configurations [2]. However, when these high-fidelity methods are utilized as a design and optimization tool, they demand high computational costs. Hybrid methods offer an interesting compromise in terms of accuracy vs. CPU cost, by decoupling the flow and acoustic calculations [3]. In these methods, the sound sources can be identified by means of classical unsteady CFD methods, which have the capability of resolving noise sources, or using a CFD method in which the sources are reconstructed. The second branch uses acoustic propagation solvers to compute the acoustic source radiation into the far-field, that is considered of great importance in aeroacoustics.

As aeroacoustic problems are, by definition, highly time dependent, and as they are governed by scales that spread over several order of magnitude, it is necessary to use sophisticated methods to predict both generation and propagation

---

[*]Post-doctorate - radouan.boukharfane@isae-supaero.fr

[†]Ass. Professor - julien.bodart@isae-supaero.fr

[‡]Professor, AIAA Member - marc.jacob@isae-supaero.fr

[§]Professor - laurent.joly@isae-supaero.fr

[¶]Research Engineer - thibault.bridel-bertomeu@cea.fr

[‖]Acoustics Engineer - thomas.node-langlois@airbus.com

of broadband noise in a reliable way. Sound generated aerodynamically can be computed using aeroacoustic analogies, all based on Lighthill's work [4]. Depending on the model chosen, the source terms can be extracted either from a volume integral or a surface integral. Curle [5] proposed an integral formulation to calculate the sound from a turbulent flow past a solid surface restricted to acoustically compact source regions. Amiet [6] developed a theory for sound radiation from the TE of a simplified airfoil that also considers non-compactness effects. Both methods require a pressure distribution on the airfoil surface as an input. Alternatively, Ffowcs and Hall [7] simplified the airfoil to a semi-infinite flat plate, solving the Lighthill equation through an approximate hard-wall Green's function with velocity-based volume source terms, while Howe [8] derived a wave equation that utilizes the vorticity as a source term over a volume integral.

Most of the models used to bridge the gap between local hydrodynamic quantities at some distance upstream of the TE and the far-field sound pressure spectrum require information about the boundary-layer characteristics and the space-time distribution of the surface pressure fluctuations. However, the flow over an airfoil is inherently complex and exhibits a variety of physical phenomena including strong pressure gradients, flow separation, and confluence of boundary layers and wakes. Among several numerical methods developed to feed the far-field acoustic models with accurate boundary-layer characteristics, large-eddy simulation (LES) offers the best promise in the foreseeable future between direct numerical simulation (DNS) and unsteady Reynolds-Averaged Navier-Stokes (RANS). It indeed provides detailed spatial and temporal information regarding a wide range of turbulence scales, which is precisely what is needed to gain better insight into the flow physics of this configuration.

The present work has been carried out within the SCONE (Simulation of Contra Rotating Open Rotor and fan broadband NoisE with reduced order modelling) project that is part of the FP7 Clean Sky Joint Undertaking of the European Union that aims at investigating the noise associated with CROR/UHBR fan technologies in order to reach optimal noise reduction. Since it is experimentally challenging to measure pressure on the surface without affecting the flow field, a computational approach is chosen. A detailed characterization of the surface pressure fluctuations provides an accurate input for current analytical approaches, thus improving the far field predictions. For this reason, the first objective of the SCONE project is to address the flow over a Controlled-Diffusion (CD) airfoil. It was originally part of an air conditioning unit developed by Valeo and was slightly re-designed to imprint on it a load similar to that of a CROR blade. The flow is computed for multiple values of Mach number, Reynolds number and angle of attack. The configuration is a replica of the experiments performed within the CRORTET Clean Sky project, to which the computational results are compared. It is worth noting that the experimental aerodynamic data are not sufficient to provide the boundary layer parameters needed to normalize the wall-pressure spectra obtained in the experiment, which shows how important LES is for proper wall pressure modelling. This present study is a first step towards a deeper quantitative investigation about the effect of varying Reynolds number, angle of attack and upstream Mach number onto the chordwise development of boundary layer characteristics.

The next sections of this article are organized as follows. Section II is devoted to describing the computational setup of the studied configurations as well as some analysis of computational resolution issues. Section III describes the global flow topology. The next part of manuscript corresponds to Sections IV and V, which provides some preliminary results. Finally, conclusions and future works are drawn in Section VI.

Computational setup

The present numerical simulations are performed with the massively parallel finite-volume solver CharLES^X for the compressible Navier-Stokes equations discretized on an unstructured grid. This code uses a finite volume approach, with second order schemes in space and low numerical dissipation associated with a third-order Runge-Kutta scheme for explicit time advancement. This solver has been applied to several airfoil studies [9, 10]. In the present study, a Vreman SGS model models the sub-grid scales [11]. The three-dimensional computational domain is meshed using an O-type topology, with a spanwise extent dictated by the maximum thickness of the boundary layer $\delta_{\max}$, for an accurate estimate of the correlation length ℓ_z. In this respect, the airfoil must span at $2\delta_{\max}$ [10, 12]. In the present study,

preliminary RANS simulations were conducted so to estimate δ_{max}, and prescribe the spanwise length L_z*. The domain extends 20 chords in all directions from the airfoil, to allow for velocity inlet boundary to act as free-stream. The size of computational domain ensures that the solution is domain-independent and the flow over airfoil surface remains unaffected by the domain boundaries. Unstructured control volume with a structured-like layer around the airfoil and unstructured elements in the far-field are used to reduce the computational costs while preserving an accurate resolution of the boundary layer (cf. Fig. 1) [†]. Prior to this simulation, coarser grid simulations were carried out to determine the resolution requirements following the recommendations of Grebert et al. [10]. In order to save computational time during the statistical convergence of the extruded 3D LES , the farfield quasi-inviscid flow is computed using a two-dimensional airfoil. Since the farfield flow is not influenced by the boundary layer developing at the wall of the airfoil (20 chords away), it is indeed assumed that initializing the farfield flow in 2D and then extrapolating into the 3D mesh allows significant time savings. Note that the two-dimensional computations are carried out on a slice of the extruded 3D mesh in order to minimize the dissipation and/or the dispersion of the farfield data upon extrapolation. The grid spacings and resolution as well as the different parameters values chosen in the present computations are summarized in Table 1.

(a)   (b)
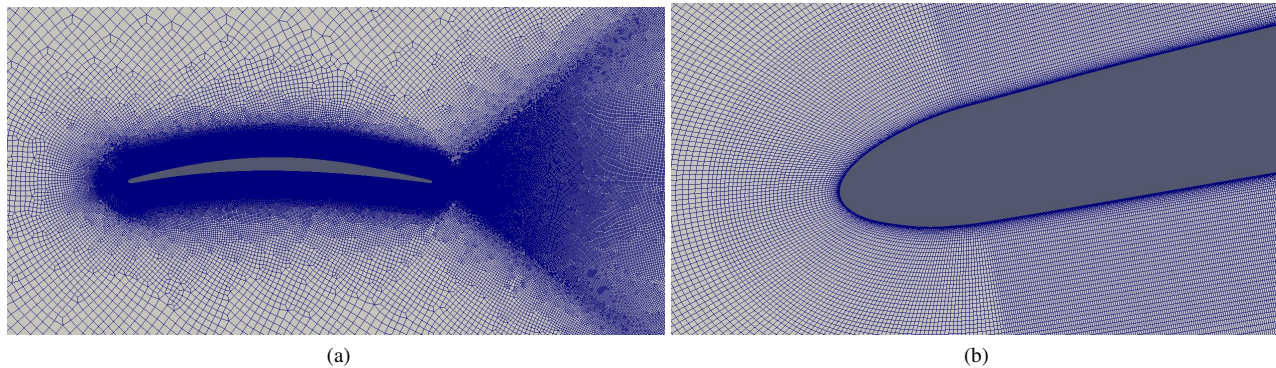
Fig. 1   Illustration of the mesh (a) Mesh around the airfoil, (b) enlargement of the mesh around the leading edge region for case C_∞.

Adiabatic boundary conditions are applied to the airfoil surface and periodic boundary conditions are used in the homogeneous, spanwise direction. As already mentioned, the three-dimensional simulation is started from a spanwise extruded two-dimensional solution. The computational time step is 1.54×10^{-5} in non-dimensional time units based on the chord length and the free-stream speed of sound to obtain a maximum CFL number regarding the RK time integration.

There exist many criteria to assess the mesh resolution quality. Some of them are based on mathematical estimates, while others rely on rather heuristic arguments. For example, the recommended orders of magnitude of computational mesh cell sizes as stated, for instance, by Piomelli and Balaras [13], Piomelli and Chasnov [14] and [15] are quite satisfactorily met (cf. Table 1). The mesh resolution quality is also assured by monitoring the Pope criterion IQ_k that represents the ratio of resolved turbulent kinetic energy to resolved plus SGS turbulent kinetic energy $IQ_k = \mathcal{K}/(\mathcal{K} + \mathcal{K}_{SGS})$. Resolved turbulence, $\mathcal{K}$, is evaluated as $(u_1'^2 + u_2'^2 + u_3'^2)/2$, where u_i' is the RMS value of fluctuating part of the velocity component u_i, while subgrid scale turbulence is estimated by $\mathcal{K}_{SGS} = (v_t/(C_M \Delta))^2$, where v_t is the kinematic turbulent viscosity, C_M a constant equal to 0.069 and Δ is estimated as the cubic root of the elements volume. Fig. 2 displays the PDF obtained with Pope's quality index. Provided that $IQ_k \geq 0.8$, the mesh

---

[*] In order to take into account the underestimate of δ_{max} by means of RANS calculations, L_z has been set to at least bigger that 2.8 δ_{max} as can be seen from Table 1.

[†] All cases have the same mesh distribution except the he height of the first mesh cell, which is calculated depending on the flow conditions to ensure $\Delta y^+ < 1$.

case	M_∞	Re_c	Angle of attack	$\delta_{\max}$	L_z	Δx^+	Δy^+	Δz^+	N_{cells}
C_1	0.3	8.30×10^5	4°	3.4% c	10% c	≤ 28	≤ 1.02	13.21	225 001 000
C_2	0.3	8.30×10^5	7°	7.1% c	20% c	≤ 27	≤ 1.04	14.03	450 987 000
C_3	0.3	2.40×10^6	7°	7.3% c	20% c	≤ 29	≤ 1.11	14.17	450 987 000
C_4	0.5	2.29×10^6	4°	3.3% c	10% c	≤ 28	≤ 1.12	13.24	225 493 500
C_5	0.5	2.29×10^6	5°	4.8% c	20% c	≤ 26	≤ 1.22	14.23	450 987 000
C_6	0.5	2.29×10^6	6°	6.1% c	20% c	≤ 24	≤ 1.20	13.28	450 987 000
C_7	0.7	2.40×10^6	1°	5.3% c	20% c	≤ 23	≤ 1.09	13.11	450 987 000

Table 1   Grid spacing and resolution along the blade surface and description of main parameters of the present computations.
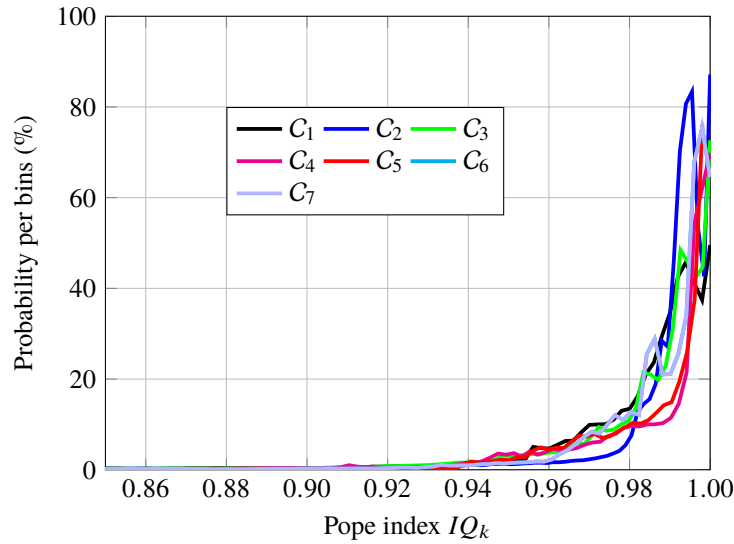

Fig. 2   PDF of the quality index IQ_k obtained in the box $[-2c, 3c] \times [-2c, 3c] \times L_z$ surrounding the CD airfoil.

resolution is considered to be sufficient since it means that at least 80% of the turbulent kinetic energy is captured at the resolved scale [16]. It can be seen that $IQ_k \geq 0.94$ for all cases, which means that the resolution level is excellent and almost reaches standard DNS resolution criteria.

Flow topology

Instantaneous Flow Field

Since the turbulent structures evolving in the turbulent boundary layer are responsible for the wall-pressure fluctuations, the first step regarding the prediction of aerodynamic noise is the identification of acoustic sources. The simulations provide detailed informations about the unsteady flow around the airfoil from which the required inputs of the trailing edge noise models are derived. The aerodynamics model inputs are indeed mean flow parameters (convection velocity) as well as second order statistics (wall pressure spectra, coherence length). An illustration of the computed flow field is shown in Fig. 3. It displays a typical instantaneous flowfield snapshot with extracted vortical structures identified by using an iso-surface of Q criterion coloured by instantaneous streamwise velocity values for case C_1. A
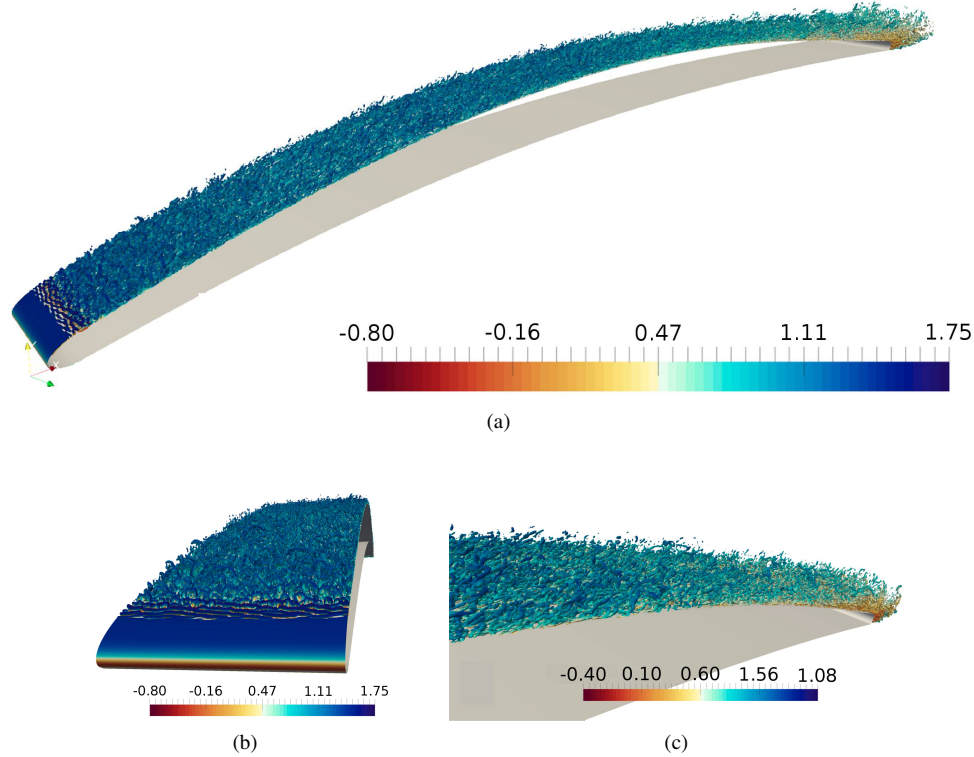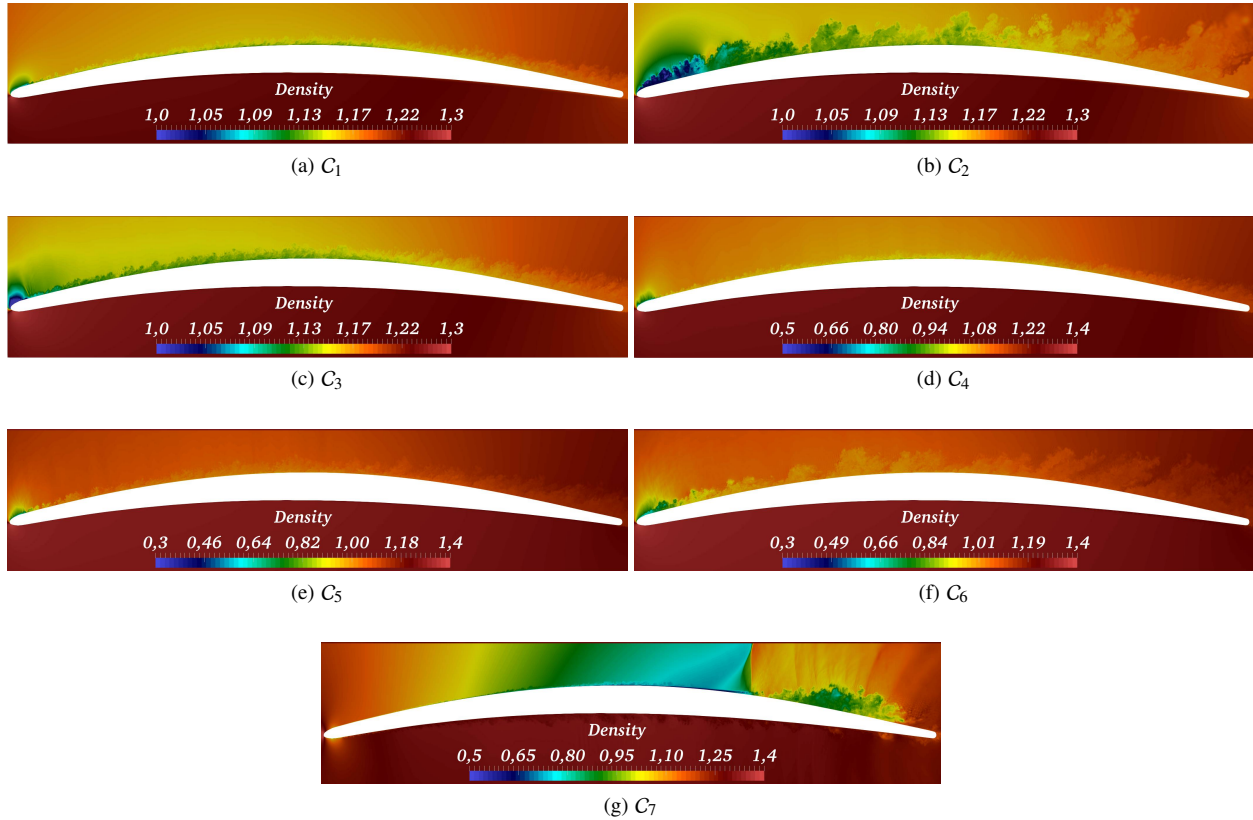
Fig. 3 Instantaneous visualization of the flow field described by the Q criterion, coloured by normalised streamwise velocity component of (a) Valeo CD airfoil, (b) zoom at the LE and (c) zoom at the trailing edge for case C_1.

laminar boundary-layer is present on the lower (pressure) side of the airfoil, and a transitional and turbulent boundary layer on the upper (suction) side. Transition from laminar to turbulent state occurs in the shear layer resulting from the flow separation in the leading edge region. It results in a massive generation of vorticity downstream of the leading edge, with large vortices shed from the suction side of the airfoil. Yet there are still some smaller vortices that remain attached to the wall and roll over the airfoil suction side and graze at the trailing edge. Eddies in the boundary layer are smaller with lower streamwise velocity values.

Fig. 4 represents the instantaneous density field for the seven studied cases. On the suction side, the turbulent boundary layer remains attached but its thickness greatly increases as the angle of attack increases (cases C_1-C_2 and C_4-C_5-C_6). The picture also demonstrates that the length of the detached shear layer in the leading edge region is significantly reduced at large Reynolds number (case C_3) in comparison with case C_2, which presents the same angle of attack. As the upstream Mach number goes higher, a weak shock starts forming on the suction side and at $M_\infty = 0.7$ (case C_7), the shock stabilizes at around 65% chord. Even if tridimensional flow structures can be identified close to the trailing edge, the shocks displacements are almost bi-dimensional and a view at mid span is representative of the major unsteady flow features.

Leading edge recirculation bubble

Another important feature of these simulations is the presence of a recirculation bubble on the suction side of the airfoils, in vicinity of the leading edge (see Fig. 5). The extent of the bubble is found to vary with the operating point. the downstream anchor point undergoes stronger variation than the upstream one. The effect of an increased angle of attack of the airfoil is clearly visible and leads to an increase of the bubble extent, more precisely to a displacement of

Fig. 4   Visualization of the instantaneous density field (normalized by the free-stream density) from 3D LES field for the three cases.

the downstream anchor point further down. The figure also shows of the bubble length with the Mach number.

Also, one can witness the effect of an increase in the upstream Mach number on the bubble, all other parameters being set. Indeed, as the upstream Mach number increases, albeit slightly, the bubble length decreases slightly. Cases C_4-C_5-C_6 show that, for conditions at which a separation bubble forms, as the angle of attack increases, the separation point moves upstream and the separation bubble length decreases, agreeing with the trends reported for other airfoil sections at high Reynolds numbers [17]. Note that case C_7 does not display any bubble on the suction side, but it can be noticed the formation of a small bubble in the pressure side.

Aerodynamic results

Fig. 6 shows the variation of the shape factor ($H_{12} = \delta^*/\theta$), the displacement thickness δ^* and the thermal boundary layer thickness δ_T against the chordwise distance x/c . The boundary layer thickness δ^* is determined as the distance from the wall to the point at which the mean streamwise (tangential) velocity (U_δ) is 99% of the free stream velocity. The thermal boundary layer thickness is derived from the classical relation $\delta_T = \delta^*/\text{Pr}^{1/3}$ verified by laminar flows with a Prandlt number Pr greater than 0.6 [18]. Near the leading edge, the flow is laminar, and the shape factor is approximately 2.6 which is a typical value of the Blasius profile (zoom not shown in this article). It can be observed that the thickness effect is associated with an increase in the length of the laminar region near the leading edge, which grows from less than 2% for the case C_1 to 10% for the case C_2. Downstream of $x/c \simeq 0.02$, the shape factor rapidly increases due to the adverse pressure-gradient and the laminar separation occurs. Then, the shape factor decreases to $H_{12} \simeq 1.6$ (larger than the typical value of the Klebanoff profile $H_{12} \simeq 1.4$ observed for turbulent boundary layers).

(a) C_1 (b) C_2

(c) C_3 (d) C_4

(e) C_5 (f) C_6

(g) C_7
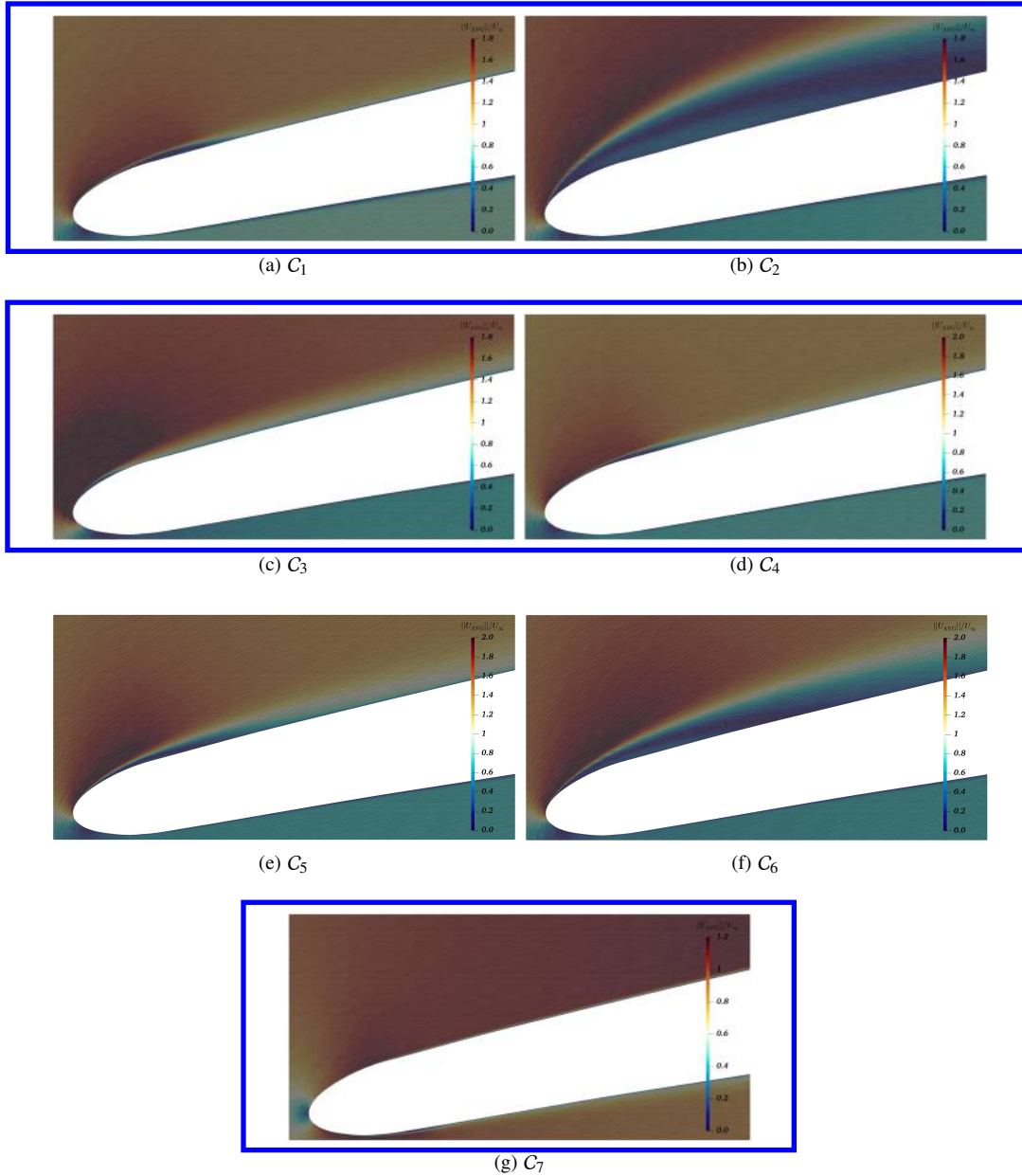
Fig. 5   Leading edge recirculation bubble found on the suction side superimposed to streamlines coloured by the magnitude of $U_{\mathrm{AVG}}/U_\infty$. Clipping is performed to highlight clearly the recirculation bubble at $x/C = 0.15$

This value depends both on the Reynolds number and the pressure gradient [19]. After the reattachment, the shape factor gradually increases, and the flow separates again in the vicinity of the trailing edge. At $0.3 \leq x/c \leq 0.5$, the flow is similar to a typical turbulent boundary layer. In this range, δ^* and δ_T almost linearly increase. Since the adiabatic wall temperature is equal to the stagnation temperature at the leading edge and thus the thermal boundary layer has the same thickness as the velocity boundary layer. Nevertheless the adiabatic wall temperature is found to be less than the stagnation temperature downstream, thus the thermal boundary layer is thicker than the velocity boundary layer as shown on Fig. 6b. The only exception is when the Mach number becomes higher (case C_7), both thermal and boundary layer thickness superimpose upstream of the shock position, whereas downstream of the shock, the thermal boundary

layer thickness is slighlty higher than the displacement thickness.

(a)

(b)
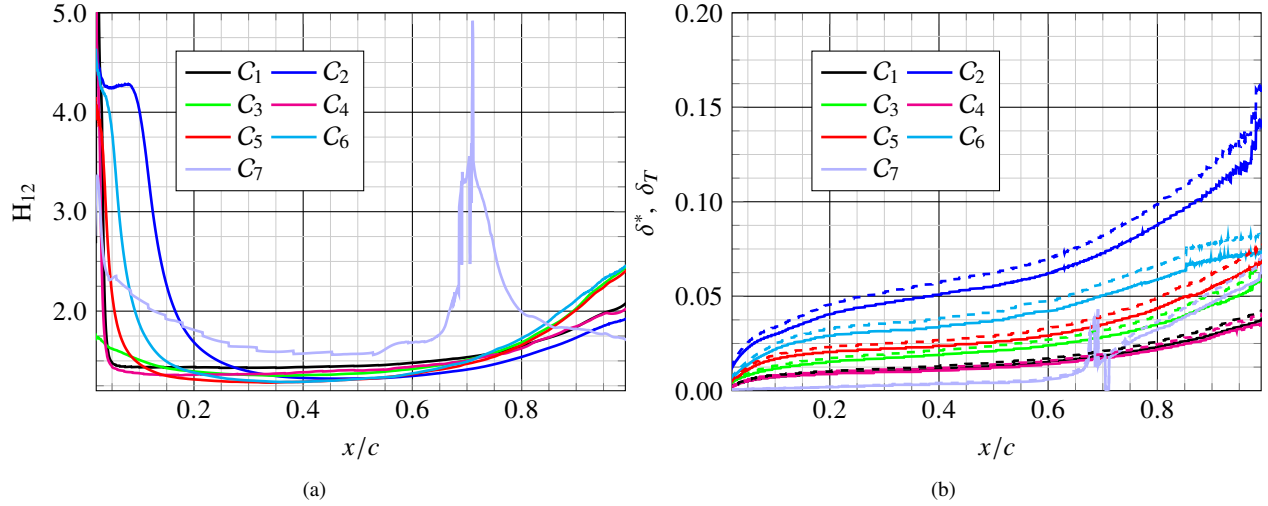
Fig. 6 Variations of shape factor $H_{12} = \delta^*/\theta$ **(a) and of displacement thickness** δ^* **(solid lines) and thermal boundary layer thickness** δ_T **(dashed lines) (b) with chordwise distance** x/c**.**

The mean static pressure distribution from the LES simulations is compared to available wind-tunnel measurements. As shown in the Fig. 7, all LES predict very accurately the distribution of the mean wall-pressure coefficient $C_p = 2(\overline{p} - p_\infty)/\rho_\infty u_\infty^2$ (where p_∞, ρ_∞ and u_∞ are farfield static pressure, density and velocity), in comparison with experimental results, and 2D LES and RANS simulations. Except minor differences observed in the recirculation region (LE) for cases C_2-C_6 and at the shock position for case C_7, 3D LES simulations are in reasonably good agreement with experiments. The profile for the 3D LES appears slightly shifted towards the leading edge but the shape is correct for the two cases where minor differences are noticed (cases C_2 and C_7). One can notice that the prediction of the leading edge laminar separation bubble and the transition, which is represented by the kink in the C_p curve, are slightly more accurately estimated by the $3D$ LES simulations for all cases.

Frequency spectra of surface pressure fluctuations

Data acquisition

A large set of numerical probes have been embedded in the first wall-normal cell along the airfoil. These probe lines are subsequently extruded in the spanwise direction in order to cover the whole computational domain. One such two-dimensional distribution is placed every 0.02% chord, leading to either 500 or 1000 repetitions in the spanwise direction, whether the spanwise length is 10% (cases C_1-C_4) or 20% chord (cases C_2-C_3-C_5-C_6-C_7), respectively. The streamwise separation of the probes is kept constant except in the vicinity of the leading and trailing edges. LES computations were run for 4 flow-through times (t_c), based on the free-stream velocity and airfoil chord length, before a statistically steady state was reached and mean values were collected. In order to remove spurious high frequencies, airfoil surface pressure and velocity statistics were then acquired over a period of 18 (cases C_1-C_4) or 15 (cases C_2-C_3-C_5-C_6-C_7) flow-through times with a normalized sampling frequency of 600 (600 pressure and velocity samples are collected per probe and convective time scale t_c).
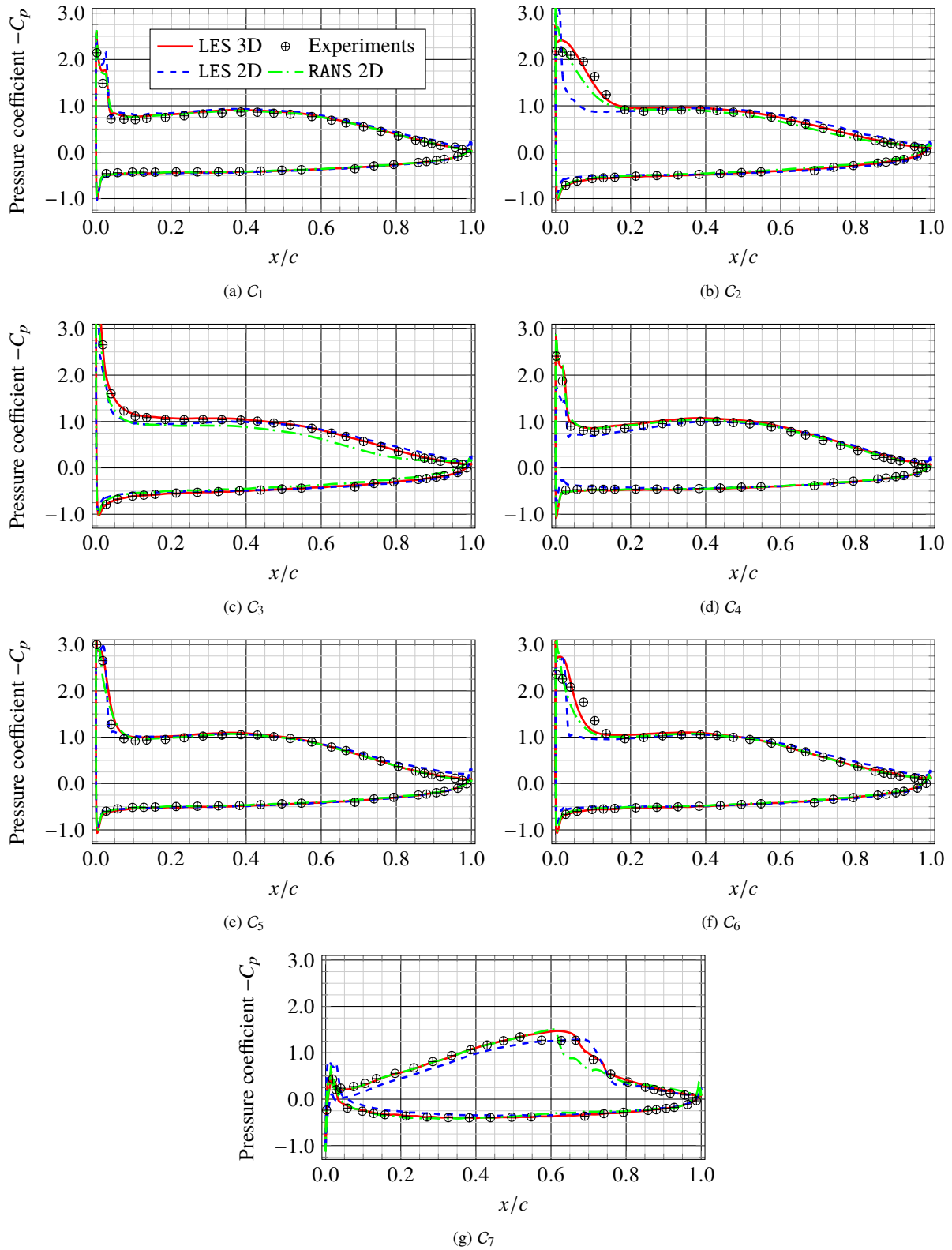
Fig. 7 Comparison of the time-averaged pressure coefficient distribution between the present LES simulation, and experimental data as well as 2D LES and RANS simulation.

Wall-pressure power spectral density

The wall pressure spectrum is one of the required inputs of Amiets theory for prediction trailing-edge noise. To estimate it, the two-point time cross-correlation function $\mathcal{R}_{p_i p_j}$ is first calculated as

$$\mathcal{R}_{p_i p_j}(\tau) = \langle p'(x_i, t) p'(x_j, t - \tau) \rangle \tag{1}$$

with τ is the time delay between the two considered signals, $p'(x_i)$ represents the surface pressure fluctuation from probe i located at x_i and $\langle \cdot \rangle$ denotes the time averaging. The cross-spectrum (*i.e.* the cross-spectral between two signals p_i and p_j) is obtained from the Fourier transform of the correlation function $\mathcal{R}_{p_i p_j}(\tau)$.

The Power Spectral Density PSD that is the Fourier transform of the autocorrelation function $\mathcal{R}_{p_i p_j}(\tau)$ of the pressure fluctuations computed near the trailing edge are compared with the measurements at two locations $x/c = 0.98$ and $x/c = 0.95$ in Fig. 8. Note that all spectral quantities are obtained using Welch's method considering segment of size $N/16$, where N is the number of sample of each case, with 50% overlap combined with the Hanning window function applied to each segments. A very good agreement is obtained for all the studied cases, although the LES results slightly under-predict the pressure fluctuations at low Strouhal number in the cases C_3-C_4-C_5 [‡]. In particular, the overall good estimate of the wall pressure fluctuations in the frequency range of interest regarding noise generation at the trailing-edge, suggests that the LES data set might be a good candidate for statistical broadband noise prediction models. The tonal peaks that arise from the experimental spectra on Fig. 8 are due to duct models of the transonic wind-tunnel facility which was not acoustically treated. The discrepancies at low frequencies may be partly due to installation effects of the experiment which are not accounted for in the simulations, but also to a lack of statistical convergence of the LES spectra as a result of the time series being short. By comparing spectra obtained for both locations, it can be concluded that very close to the trailing edge, the wall-pressure statistics are well established and almost stationary justifying the use of radiation models based on a wall-pressure statistics at a single point close to the trailing edge [6, 21]. For all cases, all spectra at both positions exhibit three distinct zones. The first one at lower Strouhal number (lower frequencies) corresponds to an almost constant power spectral density. This region extends at least up to $St = 8$ for all cases. Beyond a first cut-off frequency at about $St \sim 8 - 10$, the spectra scales close to St^{-2} for the adverse-pressure-gradient case. Moreover the size of this region increases with the boundary-layer thickness-based Reynolds number because of either a higher flow speed or angle of attack. At high frequencies, beyond a second cut-off frequency all spectra show a St^{-5} decay. This typical decay has been measured and theoretically modelled beneath two-dimensional and three-dimensional boundary layers [22] for any pressure gradients incidence [23]. At fixed Reynolds number and increasing angle of attack (cases C_1-C_2 and C_4-C_5-C_6, one can notice that the spectral content changes: the spectral hump narrows down and tones have a higher amplitude; the lower angles of attack yield typical of vortex shedding spectra, and the higher angles of attack yield the regularly decreasing spectra with a slope close to -5 almost over the whole frequency range of the decay which is typical of the turbulent boundary layer. Note that cases $\triangledown$-C_6 show at high Strouhal numbers a pile-up of energy.

Sensitivity to spanwise domain size

It is known that the coherence of pressure fluctuations decays faster in the spanwise direction than in the streamwise direction, indicating that the spanwise coherence length scale in the pressure field is a key parameter in models for trailing edge noise prediction [24]. Indeed, it determines how the noise radiated by TEsources distributed along the span adds up and thus has a direct influence onto the overall TE-source efficiency and resulting noise level. Therefore, an evaluation of the coherence length is required to predict the Sound Pressure Level SPL radiated by the airfoil. Accurate measurements of this length scale rely on a sufficient extension of the spanwise domain for the frequency range of

---

[‡]It is important to note at this stage that the simulation parameters (grid resolution, SGS model, Boundary condition) required for an accurate prediction of fluctuating wall pressure are more stringent relative to those necessary for predicting the main profiles (as pressure coefficient C_p). As for the need of a good grid resolution, the reader is referred to study of Park and Moin [20] who identified the resolution requirements for predicting the low frequency content of fluctuating wall pressure in a turbulent channel flow.

(a) C_1

(b) C_2

(c) C_3

(d) C_4

(e) C_5

(f) C_6

(g) C_7
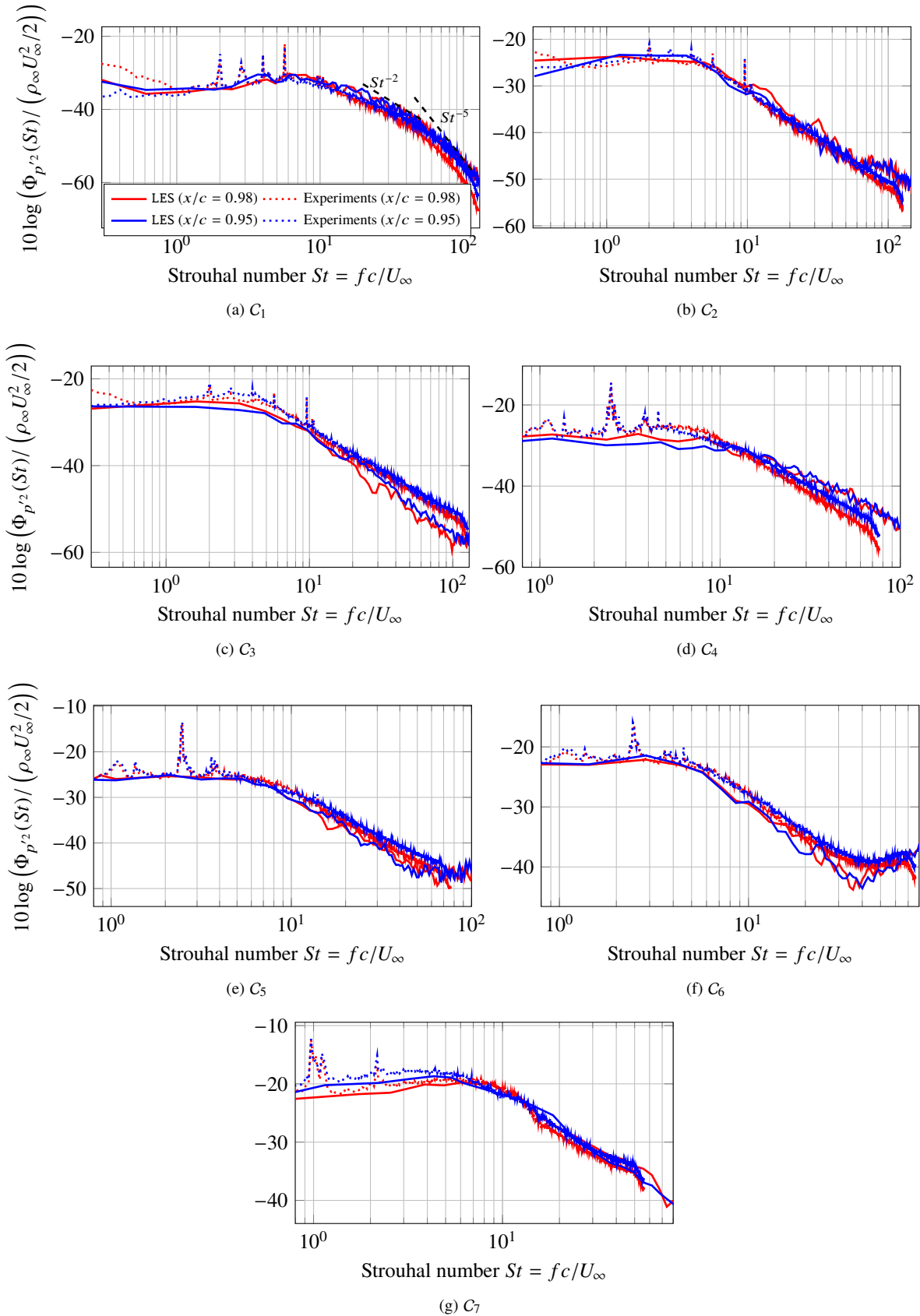
Fig. 8   Wall-pressure power spectral density at $0.2\%c$ **and** $0.5\%c$ **upstream of the trailing edge.**

interest which is difficult to achieve numerically. In fact, for all cases only a portion of the airfoil span was simulated and the flow was assumed to be homogeneous in the spanwise direction. In a statistical sense, the size of a coherent source region around a spanwise position z is estimated using the coherence function [25]

$$\gamma^2(z, \Delta z, f) = \frac{|\Phi_{pp}(z, \Delta z, f)|}{|\Phi_{pp}(z, 0, f)||\Phi_{pp}(z + \Delta z, 0, f)|} \tag{2}$$

where Φ_{pp} is the cross spectrum function. The coherence function γ^2 is computed from the fluctuating surface pressure p' in the vicinity of the trailing edge. If the spanwise distribution is homogeneous, the cross spectrum does not depend on z. Thus, if in Eq.(2) the streamwise separation is fixed, the cross-spectrum only depends on the separation Δz between consecutive points. The spanwise coherence at a location close to the trailing edge ($x/c = 0.98$) is plotted for the suction side in Fig. 9. The spanwise coherence of the wall pressure fluctuations decays over a distance that is shorter than the spanwise extent of the computational domain sufficiently, even at low frequencies, by mid-span within the range of frequencies over which experimental data is available. This indicates that the current spanwise computational domain size is large enough to capture a statistically independent acoustic source region and to compute the coherence length scales; both are key input parameters to noise predictions. In other words, sources separated by distances larger than the simulated half-span radiate sound independently in a statistical sense. Therefore, the broadband noise measured by the microphone can be compared to the LES -Amiet noise predictions after scaling the latter up by a factor of $10 \log_{10}(L_{exp}/L_z)$ where L_{exp} is the spanwise length of the airfoil model in the experiment.

In Fig. 10, a comparison is made between the experimental and computed values of the spanwise coherence of fluctuating surface pressure at the near trailing edge $x/c = 0.98$. The LES results are show to predict quite satisfactorily the higher frequency behaviour of the coherence but not the low frequency value except for the spurious tones that appear in the experimental data and the very low frequencies that are flawed both in the experiment (installation effect) and in the CFD (length of times series, limited spanwise extent). One can not that the coherence at low frequencies is extremely sensitive to sample size and numerical errors [26].
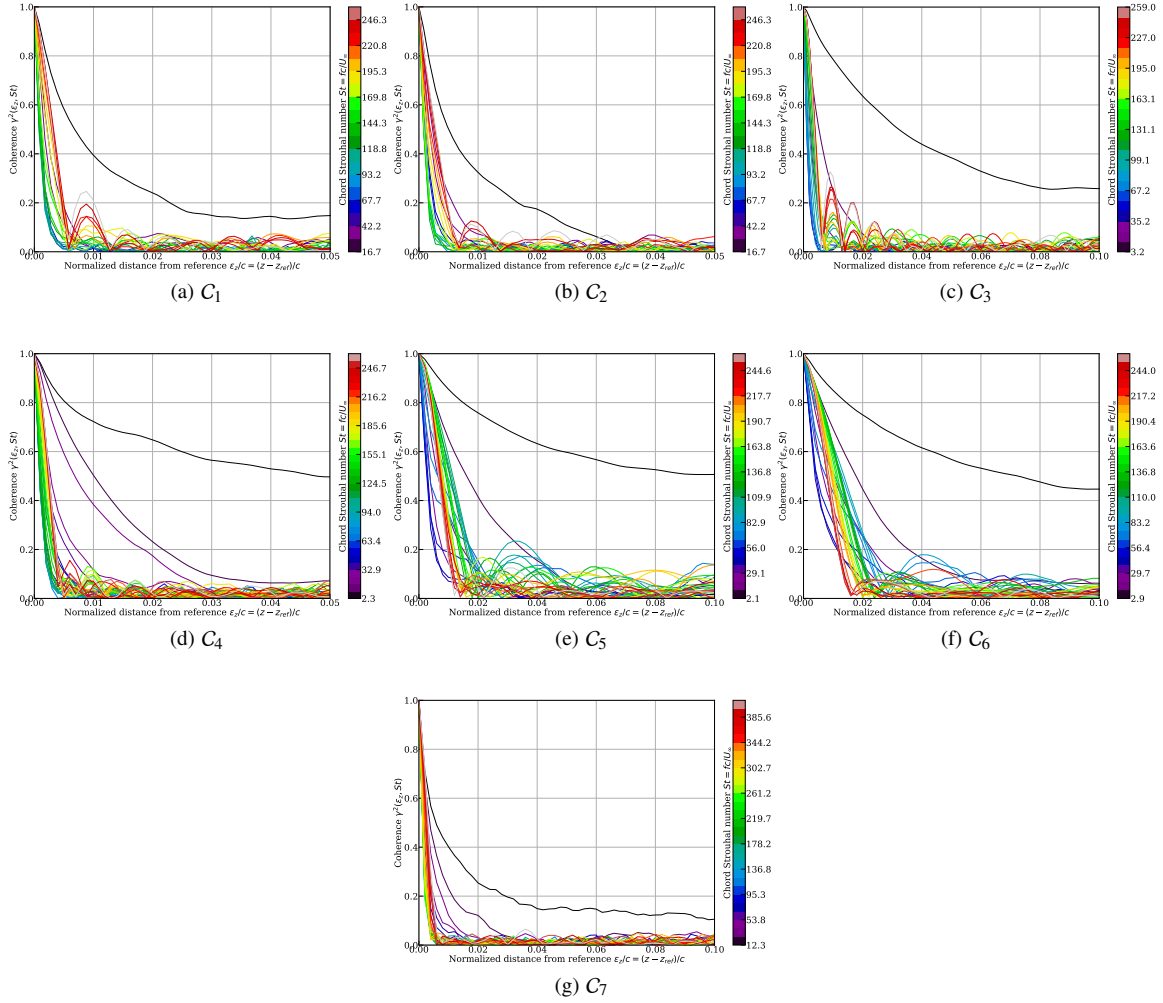
Spanwise coherence length

Through classical diffraction theory [6], an estimation of the acoustic power spectra is found to be proportional to the coherence length. By definition, the length scale is related to the integral of the square root of the coherence function γ^2 over its spatial coordinate and therefore reduces to a function of frequency only if the spanwise distribution is assumed to be homogeneous:

$$\ell_z(f) = \lim_{L \to \infty} \int_0^L \sqrt{\gamma^2(\Delta z, f)} \mathrm{d}(\Delta z) \tag{3}$$

Two models have been selected for comparison. Amiet [6] suggests the use of an expression based on Corcos [27] work for the spanwise coherence length of a flat plat turbulent boundary layer at equilibrium, $\ell_z \approx bU_c/f$ under the assumption that the normalised cross-power spectral density $\Phi_{pp}(z, 0, f)/\Phi_{pp}(0, 0, f)$ can be represented by a function depending on a single dimensionless variable $B(fa/U_c)$. The constant can be approximated as $b \approx 2.1$ and the characteristic convection velocity U_c shows only a weak dependency on the frequency. This model has been proven to give good approximation of ℓ_z for high frequencies.

Salze et al. [28] developed a model based on Efimtsov [29] to correctly evaluate ℓ_z over the whole, especially low-frequency scales, by introducing boundary layer thickness dependence:

$$\ell_z = \delta^* \left[\left(\frac{a_1 f \delta^* U_\infty}{cU_c} \right)^2 + \frac{a_2^2}{f\delta^*(H_{12}^2 U_\infty/u_\tau)^2/c + (a_2/a_3)^2} \right]^{-1/2} \tag{4}$$

Fig. 9 Spanwise coherence of the simulated surface pressure fluctuations on the CD airfoil at suction side $x = 0.98c$ **for the entire range of frequencies over which far-field noise measurements are available.**

where u_τ is the friction velocity, and parameters a_1, a_2 and a_3 are defined specifically for the streamwise and cross stream directions. As it has been reported by Palumbo [30], the nominal values a_1, a_2 and a_3 have to be modified to obtain the right length scales. The latter model is constrained by the Corcos model [27] (through a_1) at mid to high frequencies, while parameter a_2 controls the frequency at which th Efimtsov model breaks away from the Corcos curve. The last parameter a_3 controls the low frequency roll off. The frequency and height of the peak in the coherence length curve can then be set by adjusting a_1, a_2 and a_3. In the present study, the value of U_c/U_∞ has been fixed to 0.69 and the parameters a_1, a_2 and a_3 have been estimated for each case to fit as much as possible the calculated coherence length curve.

The spanwise coherence results obtained from the LES computations as well the fit of the Corcos [27] and Efimtsov models [28] are shown in Fig. 11. The fit is a compromise in that some error must be tolerated at the high frequencies in order to reasonably match the low frequency hump. Note that depending on the studied cases, the fitting procedure returns slightly different values for a_2 and similar values of a_1 and a_3. The a_2 parameter had to increased when increasing Mach number (recall that the case C_7 presents a shock wave).
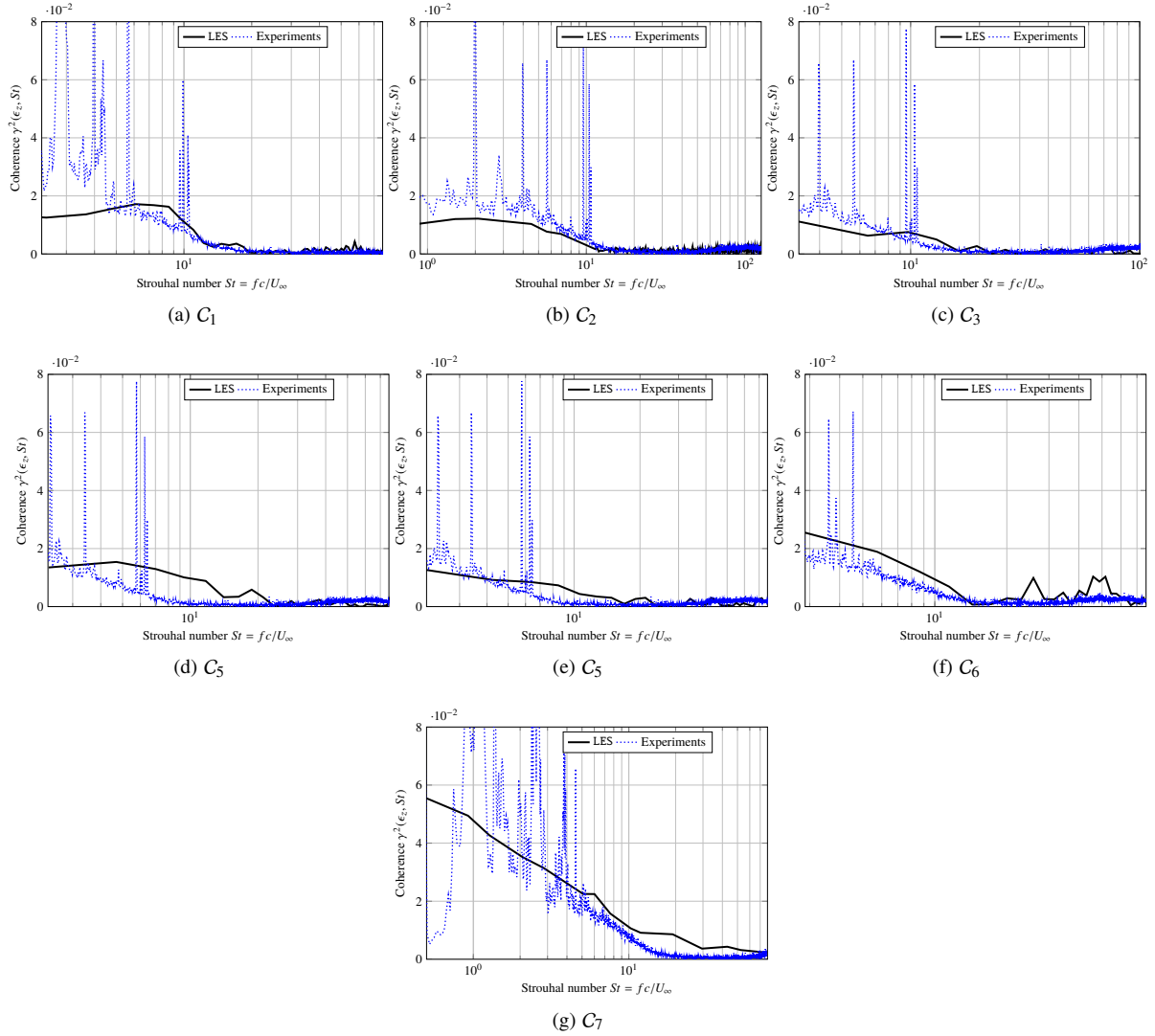
Fig. 10 **Spanwise coherence at 2%c upstream of the trailing edge.**

Conclusions and work in progress

The large-eddy simulation of the Valeo CD airfoil has been described and compared with some experimental results. The geometrical simplicity of this configuration allows for detailed measurements and comparisons, while representing flow phenomena relevant to practical turbomachines as far as broadband trailing edge noise is concerned. Several criteria are used to check if the resolution is fine enough to capture the flow accurately. It is shown that good results have been achieved by an adequate set-up of the LES , even for large Reynolds and Mach numbers associated to the present flow. The present LES reproduces all qualitative features of the flow found in the experiment. The evolution of the boundary layer thickness seems to be well captured. Computed wall-pressure spectra and spanwise coherence lengths are found to agree very well with the experimental spectra, regarding both amplitudes and slopes. The sensitivity to the spanwise domain size has been assessed to obtain a fully developed boundary independent flow in the spanwise direction, thus the three-dimensional flow patterns are representative of those found on large span airfoils. The computed spanwise correlation length ℓ_z has been compared to Corcos' [27] and Efimtsov model [28]. Efimtsov model [28] has been shown to provide a good estimate ℓ_z over the entire frequency range and accounts very well for the effect
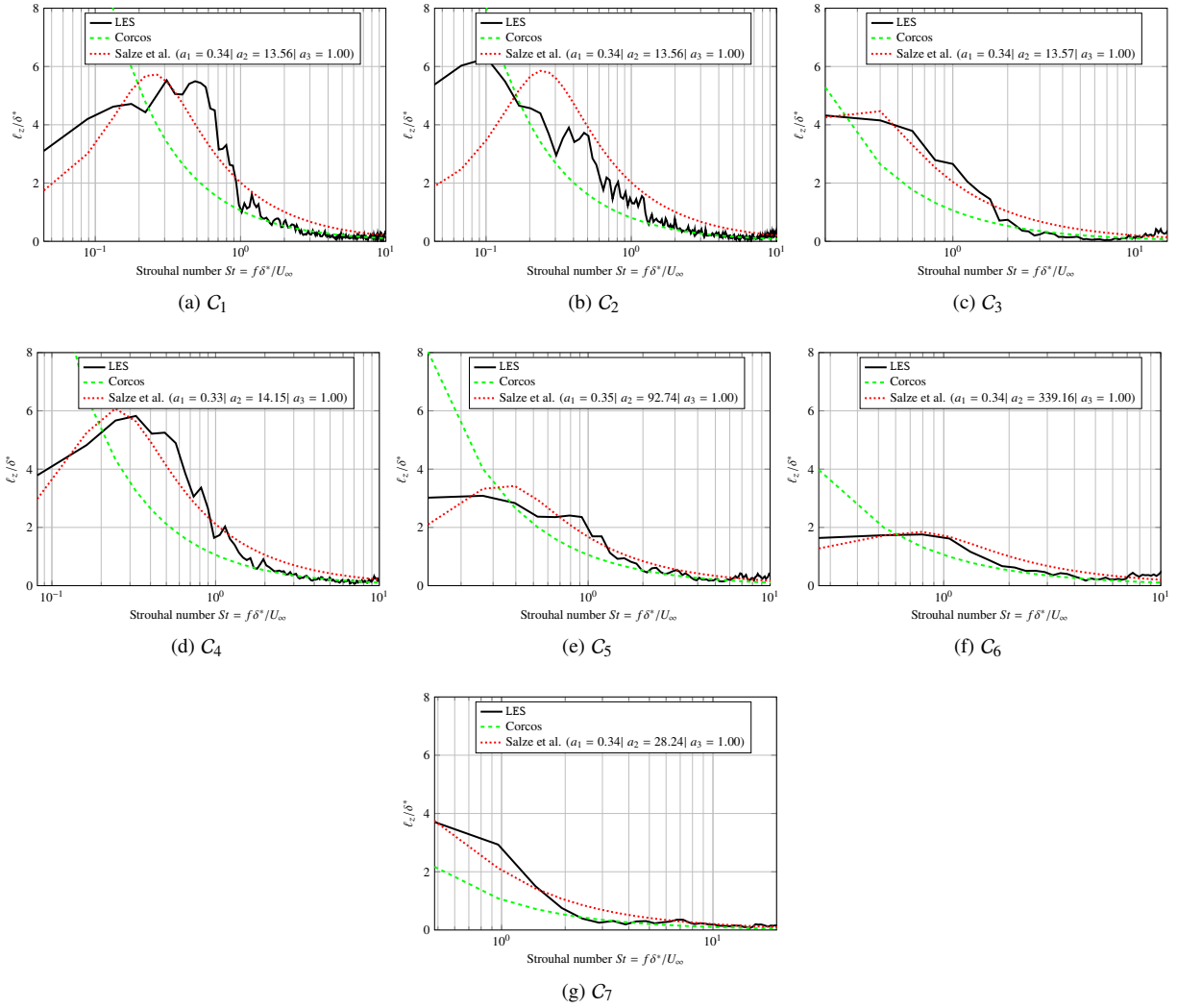
Fig. 11   Spanwise coherence length at 2%c upstream of the trailing edge.

of the pressure gradient, but it needs to be adjusted via a model constants $a_{1,2,3}$ in order to take into account Mach number effect. The quality of the results is promising for the perspectives of this work, regarding analytical sound prediction models. The present LES computations are expected to allow for a detailed analysis of the 3D turbulent flow in relation with the far field and should be beneficial for the developments of new versions of trailing edge noise models properly extended to highly loaded airfoils or compressible boundary layers. The next steps will be to assess the effects of the dynamic sub-grid viscosity and wall-modelling on the predicted wall pressure spectra. The grid also needs to be further optimized, especially in the vicinity of the leading edge to predict more properly the trigging of boundary layer transition to match the experimental C_p distribution. Parallel investigations of wall models that are currently carried out that should also shed some light on the capability of performing LES on coarser grids as needed for fast simulations on cheaper PC workstations and therefore bringing LES within reach of industrial design.

Acknowledgement

References

[1] Moriarty, P., and Migliore, P. G., *Semi-empirical aeroacoustic noise prediction code for wind turbines*, National Renewable Energy Laboratory Golden, CO, 2003.

[2] Sandberg, R. D., and Sandham, N. D., "Direct numerical simulation of turbulent flow past a trailing edge and the associated noise generation," *Journal of Fluid Mechanics*, Vol. 596, 2008, pp. 353–385.

[3] Redonnet, S., "Aircraft noise prediction via aeroacoustic hybrid methods - development and application of onera tools over the last decade : some examples." *AerospaceLab*, 2014, pp. p. 1–16.

[4] Lighthill, M. J., "On sound generated aerodynamically I. General theory," *Proc. R. Soc. Lond. A*, Vol. 211, No. 1107, 1952, pp. 564–587.

[5] Curle, N., "The influence of solid boundaries upon aerodynamic sound," *Proc. R. Soc. Lond. A*, Vol. 231, No. 1187, 1955, pp. 505–514.

[6] Amiet, R. K., "Noise due to turbulent flow past a trailing edge," *Journal of Sound and Vibration*, Vol. 47, No. 3, 1976, pp. 387–393.

[7] Ffowcs, W., and Hall, L. H., "Aerodynamic sound generation by turbulent flow in the vicinity of a scattering half plane," *Journal of Fluid Mechanics*, Vol. 40, No. 4, 1970, pp. 657–670.

[8] Howe, M. S., "Trailing edge noise at low Mach numbers," *Journal of Sound and Vibration*, Vol. 225, No. 2, 1999, pp. 211–238.

[9] Bodart, J., Larsson, J., and Moin, P., "Large eddy simulation of high-lift devices," *21st AIAA Computational Fluid Dynamics Conference, Paper n° 2013-2724*, 2013.

[10] Grebert, A., Bodart, J., and Joly, L., "Investigation of wall-pressure fluctuations characteristics on a NACA0012 airfoil with blunt trailing edge," *22nd AIAA/CEAS Aeroacoustics Conference, Paper n° 2016-2811*, 2016.

[11] Vreman, A. W., "An eddy-viscosity subgrid-scale model for turbulent shear flow: Algebraic theory and applications," *Physics of Fluids*, Vol. 16, No. 10, 2004, pp. 3670–3681.

[12] Zhang, W., and Samtaney, R., "Assessment of spanwise domain size effect on the transitional flow past an airfoil," *Computers & Fluids*, Vol. 124, 2016, pp. 39–53.

[13] Piomelli, U., and Balaras, E., "Wall-layer models for large-eddy simulations," *Annual review of fluid mechanics*, Vol. 34, No. 1, 2002, pp. 349–374.

[14] Piomelli, U., and Chasnov, J. R., "Large-eddy simulations: theory and applications," *Turbulence and transition modelling*, Springer, 1996, pp. 269–336.

[15] Pope, S. B., "Turbulent flows," , 2001.

[16] Pope, S. B., "Ten questions concerning the large-eddy simulation of turbulent flows," *New journal of Physics*, Vol. 6, No. 1, 2004, p. 35.

[17] Sepúlveda, J. A. S., "High reynolds numbers turbulent boundary layers," Ph.D. thesis, Universidad Politécnica de Madrid, 2014.

[18] Pohlhausen, E., "Der Wärmeaustausch zwischen festen Körpern und Flüssigkeiten mit kleiner Reibung und kleiner Wärmeleitung," *ZAMM-Journal of Applied Mathematics and Mechanics/Zeitschrift für Angewandte Mathematik und Mechanik*, Vol. 1, No. 2, 1921, pp. 115–121.

[19] Cousteix, J., *Aérodynamique: Turbulence et Couche Limite*, Cépaduès-editions, 1989.

[20] Park, G. I., and Moin, P., "Space-time characteristics of wall-pressure fluctuations in wall-modeled large eddy simulation," *Bulletin of the American Physical Society*, Vol. 59, 2014.

[21] Roger, M., and Moreau, S., "Back-scattering correction and further extensions of Amiet's trailing-edge noise model. Part 1: theory," *Journal of Sound and Vibration*, Vol. 286, No. 3, 2005, pp. 477–506.

[22] Goody, M. C., and Simpson, R. L., "Surface pressure fluctuations beneath two-and three-dimensional turbulent boundary layers," *AIAA journal*, Vol. 38, No. 10, 2000, pp. 1822–1831.

[23] Cipolla, K., and Keith, W., "Effects of pressure gradients on turbulent boundary layer wave number frequency spectra," *AIAA journal*, Vol. 38, No. 10, 2000, pp. 1832–1836.

[24] Rozenberg, Y., Roger, M., and Moreau, S., "Rotating blade trailing-edge noise: Experimental validation of analytical model," *AIAA Journal*, Vol. 48, No. 5, 2010, pp. 951–962.

[25] Christophe, J., Anthoine, J., and Moreau, S., "Trailing edge noise of a controlled-diffusion airfoil at moderate and high angle of attack," *15th AIAA/CEAS Aeroacoustics Conference, Paper n° 2009-3196*, 2009.

[26] Kocheemoolayil, J. G., and Lele, S. K., "Large Eddy Simulation of Airfoil Self-Noise at High Reynolds Number," *22nd AIAA/CEAS Aeroacoustics Conference*, 2016, p. 2919.

[27] Corcos, G., "The structure of the turbulent pressure field in boundary-layer flows," *Journal of Fluid Mechanics*, Vol. 18, No. 3, 1964, pp. 353–378.

[28] Salze, É., Bailly, C., Marsden, O., Jondeau, E., and Juvé, D., "An experimental characterisation of wall pressure wavevector-frequency spectra in the presence of pressure gradients," *20th AIAA/CEAS Aeroacoustics Conference, Paper n° 2014-2909*, 2014.

[29] Efimtsov, B., "Characteristics of the field of turbulent wall pressure-fluctuations at large reynolds-numbers," *Soviet Physics Acoustics-USSR*, Vol. 28, No. 4, 1982, pp. 289–292.

[30] Palumbo, D., "Determining correlation and coherence lengths in turbulent boundary layer flight data," *Journal of Sound and Vibration*, Vol. 331, No. 16, 2012, pp. 3721–3737.